

Short communication

Ionic conductivity of $\text{Li}_x\text{B}_{1-x/3}\text{PO}_4$ ceramic electrolyte based on defect models

Tae Jung Kim^a, Hee-Soo Moon^a, Seung Won Lee^a, Jong-Wan Park^{a,b,*}

^a Division of Materials Science and Engineering, Hanyang University, 17, Haengdang-dong, Seongdong-ku, Seoul 133-791, South Korea

^b Research Center for Energy Conversion and Storage, San 56-1, Shilim-dong, Kwanak-gu, Seoul 151-742, South Korea

Received 11 February 2003; accepted 13 March 2003

Abstract

The ionic conductivity of $\text{Li}_x\text{B}_{1-x/3}\text{PO}_4$ is investigated in terms of defect models with a lithium doping level of $0 < x < 0.3$. The crystalline solid electrolytes, $\text{Li}_x\text{B}_{1-x/3}\text{PO}_4$, are synthesized by a soft-chemical route by using H_3BO_3 , H_3PO_4 , $\text{LiOH}\cdot\text{H}_2\text{O}$. To determine the changes in ionic conductivity and activation energy of $\text{Li}_x\text{B}_{1-x/3}\text{PO}_4$ with lithium content x , AC-IS measurements are performed at temperatures between 25 and 90 °C. The maximum ionic conductivity is $3.74 \times 10^{-6} \text{ S cm}^{-1}$ at room temperature for $x = 0.10$, and the activation energy increases from 0.3039 to 0.3385 eV with increasing lithium content.

© 2003 Elsevier Science B.V. All rights reserved.

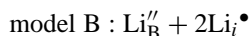
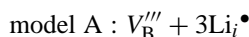
Keywords: Solid electrolyte; Ionic conductivity; Lithium battery

1. Introduction

Conventional lithium battery systems contain a liquid electrolyte, generally a concentrated organic solution of a lithium salt. The liquid state offers good contact with the solid electrodes, as well as an ionic conductivity which is slightly temperature dependent and allows stable performance between -20 and $+60$ °C. On the other hand, lithium cations, and their associated counter anions and solvent molecules are mobile and give rise to the formation of passivation layers at the electrode|electrolyte interfaces. The use of a solid electrolyte may overcome this limitation [1].

Recently, Kelder and coworkers [2,3] have shown that Li-doped BPO_4 can be used as a ceramic electrolyte for Li-ion batteries. The structures of pure BPO_4 - and MPO_4 -type compounds (where $\text{M} = \text{B}, \text{Al}, \text{Fe}$) have a continuous three-dimensional framework, analogous to the appropriate SiO_2 polymorph. In the BPO_4 structure, both boron and phosphorus atoms replace silicon and remain in tetrahedral coordination. Therefore, the structure is built up of BO_4 and PO_4 tetrahedra [4,5].

Defect models of $0.5 \times \text{Li}_2\text{O}-\text{BPO}_4$ derived by Jak et al. [6] are shown in Fig. 1 and are identified by the Kröger–Vink notation, i.e.



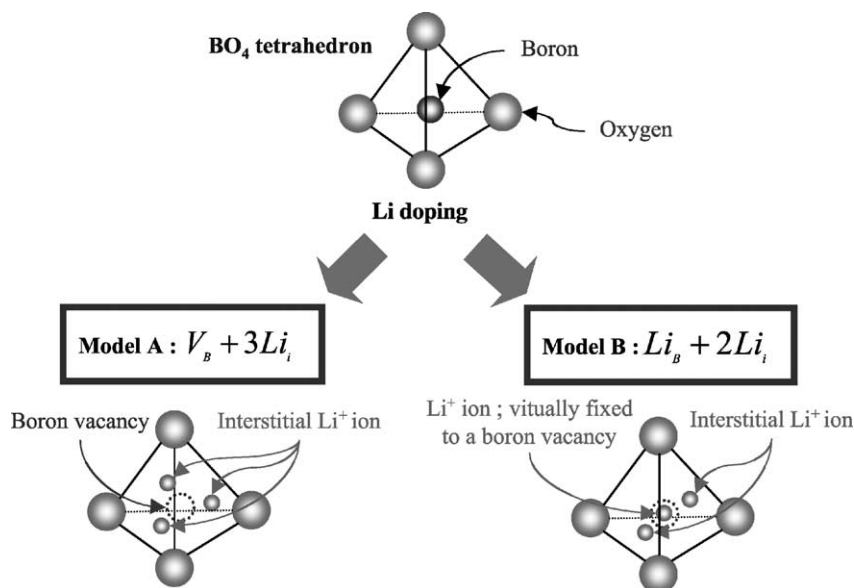
In model A, the boron vacancy is surrounded by three interstitial Li^+ -ions. In model B, one Li^+ -ion is virtually fixed to a boron vacancy and surrounded by two interstitial Li^+ -ions. According to the defect models, the conduction mechanism of $0.5 \times \text{Li}_2\text{O}-\text{BPO}_4$ is the migration of interstitial lithium ion through the boron vacancies.

The ionic conductivity is influenced by the following two factors. One is the mobile ion concentration, which is related to the concentration of interstitial lithium ions and boron vacancies. The other factor is the activation energy which is determined by the bottleneck size for the ionic conduction. This study examines the ionic conductivity of $\text{Li}_x\text{B}_{1-x/3}\text{PO}_4$ based on defect models with lithium doping levels in the range $0 < x < 0.3$.

2. Experimental

The crystalline $\text{Li}_x\text{B}_{1-x/3}\text{PO}_4$ was prepared by a soft-chemical route using H_3PO_4 (Aldrich, 99.999%, 85 wt.% solution in water), H_3BO_3 (Aldrich, 99.99%) and $\text{LiOH}\cdot\text{H}_2\text{O}$ (Aldrich, 99.995%). Stoichiometric amounts of H_3PO_4 and H_3BO_3 were mixed in de-ionized water, and appropriate amounts of $\text{LiOH}\cdot\text{H}_2\text{O}$ were added. In order to form homogeneous slurries, the mixtures were stirred for

* Corresponding author. Tel.: +82-2-2290-0386; fax: +82-2-2298-2850.
E-mail address: jwpark@hanyang.ac.kr (J.-W. Park).

Fig. 1. Defect models of $0.5 \times \text{Li}_2\text{O}-\text{BPO}_4$.

24 h. The slurries were heated in air using a box furnace at 300°C for 2 h. The products were ground in mortar and pestle in order to make fine line powders.

X-ray diffraction patterns of the powdered samples were obtained with an X-ray diffractometer (Rigaku) with $\text{Cu K}\alpha$ radiation. The diffraction data were collected at 0.02° step widths over a 2θ range from 20 to 60° . The morphology and particle size of the powders were observed by means of field emission scanning electron microscopy (FESEM).

Pellets of 10 mm diameter and with a thickness of 1–1.5 mm were prepared for conductivity measurements by cold-pressing line powder at 100 MPa. The pellets were sintered at 600°C for 4 h in order to increase their mechanical strength and minimize grain boundary resistance. For AC-IS measurements, Mo was sputtered on the two faces of the pellet as blocking electrodes. Ionic conductivity was determined from ac impedance measurements using a EG&O M6310 installment over a frequency range between 10 MHz and 100 kHz.

3. Results and discussion

X-ray diffraction (XRD) analysis revealed the $\text{Li}_x\text{B}_{1-x/3}\text{PO}_4$ to be single phase and to have a cristobalite structure regardless of the lithium content (Fig. 2). Comparison with pure BPO_4 shows the absence of a second phase and a superstructure which contains lithium ions or boron vacancies. This indicates that the interstitial lithium ions are randomly distributed over the available lattice sites. The charge-compensating boron vacancies and the substitutionally incorporated lithium ions on boron sites are also randomly distributed [7]. A low-intensity second

phase $\text{BPO}_4 \cdot 3\text{H}_2\text{O}$ peak is observed at a diffraction angle of around 28° [2,8].

FESEM micrographs show $\text{Li}_x\text{B}_{1-x/3}\text{PO}_4$ to be strongly agglomerated with primary particle sizes of 27–28 nm. In crystalline electrolytes, ionic conductivity is affected by particle size because the bulk conductivity is determined by both the grain interior conductivity and the grain boundary conductivity. Jak et al. [9] reported that the total Li^+ -ion conductivity increases with decreasing particle size. In the present study, however, the primary particle size of $\text{Li}_x\text{B}_{1-x/3}\text{PO}_4$ does not vary with lithium doping level. Thus, the influence of grain boundary conductivity on total conductivity is not considered (Fig. 3).

A representative impedance diagram plotted in the Nyquist complex plane at room temperature is shown in

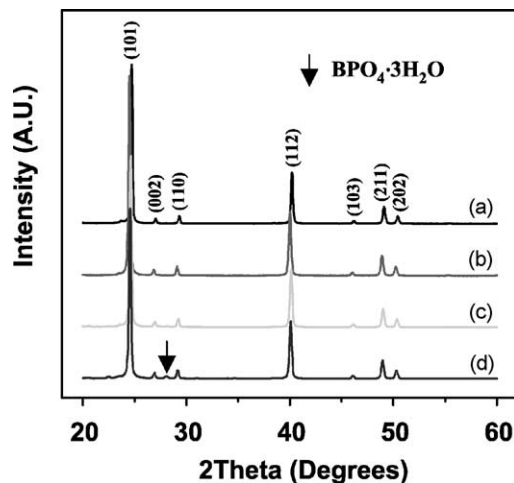


Fig. 2. X-ray diffraction patterns for $\text{Li}_x\text{B}_{1-x/3}\text{PO}_4$: (a) $x = 0$; (b) $x = 0.1$; (c) $x = 0.2$; (d) $x = 0.3$.

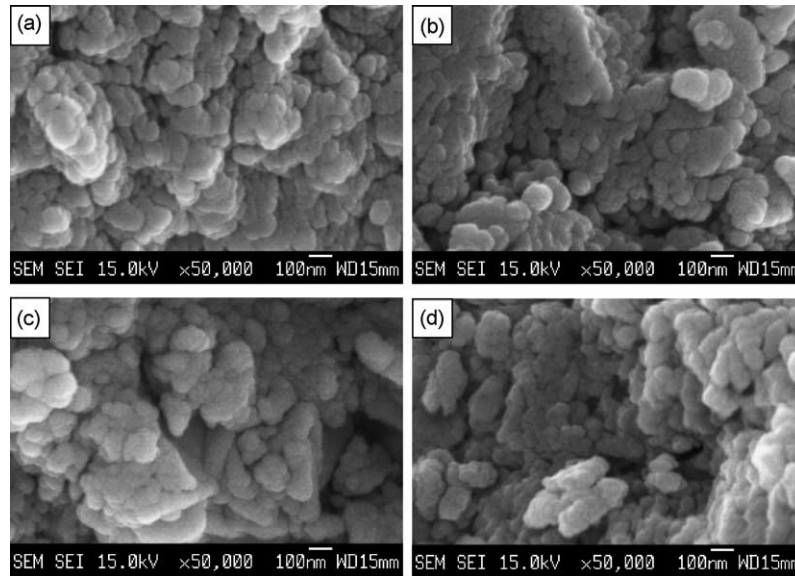


Fig. 3. FESEM micrographs of $\text{Li}_x\text{B}_{1-x/3}\text{PO}_4$: (a) $x = 0$; (b) $x = 0.1$; (c) $x = 0.2$; (d) $x = 0.3$.

Fig. 4. At high frequencies, a semicircle is present as a result of a parallel combination of bulk resistance (R_b) and capacitance (C_b). The bulk resistance includes both the grain interior resistance (R_{gi}) and the grain boundary resistance (R_{gb}). These two components are not separated in all samples. At low frequencies, there is inclined line at an approximate 45° angle to the real axis, i.e. the Warburg impedance. This is part of the interfacial impedance and is due to an electrode contribution. The behavior of the impedance plots shows characteristics of a pure ionic conductor composed of bulk and electrode contributions [10].

The changes in bulk resistance, capacitance and ionic conductivity of the $\text{Li}_x\text{B}_{1-x/3}\text{PO}_4$ with lithium content x is shown in Table 1. The capacitance is calculated from the frequency at the maximum of the semi-circle and the con-

ductivity is obtained from the value of the intercept of the extrapolated high-frequency semi-circle with the real axis. The capacitance is of the order of 10^{-11} F which is a typical value for the bulk capacitance [11]. With increasing x the conductivity increases reaches a maximum value, and then decreases. The maximum ionic conductivity is $3.74 \times 10^{-6} \text{ S cm}^{-1}$ at room temperature for $x = 0.10$. Usually, the ionic conductivity is given by:

$$\sigma_1 = qc_i\mu_i = \frac{\sigma_0}{T} \exp\left(\frac{-E_a}{kT}\right) \quad (1)$$

where q is the ionic charge, c_i the carrier concentration, μ_i the mobility of the ion, σ_0 the pre-exponential factor, E_a the activation energy, k the Boltzman constant. The ionic conductivity depends on the carrier concentration and mobility.

The pre-exponential term is related to the carrier concentration and the activation energy is related to carrier mobility. It is possible to consider the maximum conductivity as the combination of high carrier concentration and low activation energy.

To investigate the activation energy of $\text{Li}_x\text{B}_{1-x/3}\text{PO}_4$ with lithium content x , AC-IS measurements were performed between 25 and 90°C . A plot of $\ln(\sigma T)$ as a function of $1000/T$ for $x = 0.1, 0.2$ and 0.3 , is presented in Fig. 5. The conductivity follows the Arrhenius law

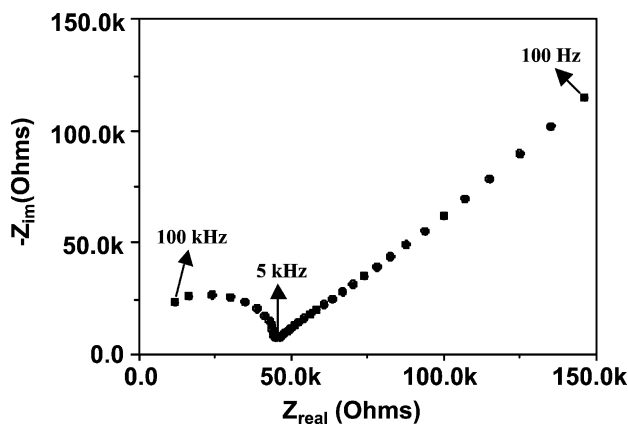


Fig. 4. Complex impedance diagram of $\text{Li}_x\text{B}_{1-x/3}\text{PO}_4$ ($x = 0.10$) at room temperature.

Table 1

Value of bulk resistance (R_b), capacitance (C_b) and ionic conductivity ($\sigma_{25^\circ\text{C}}$) with different lithium contents (x)

x	R_b (Ω)	C_b (F)	$\sigma_{25^\circ\text{C}}$ ($\Omega^{-1} \text{ cm}^{-1}$)
0.10	95410	1.85×10^{-11}	3.74×10^{-6}
0.20	265900	2.99×10^{-11}	1.34×10^{-6}
0.30	370800	2.15×10^{-11}	9.63×10^{-7}

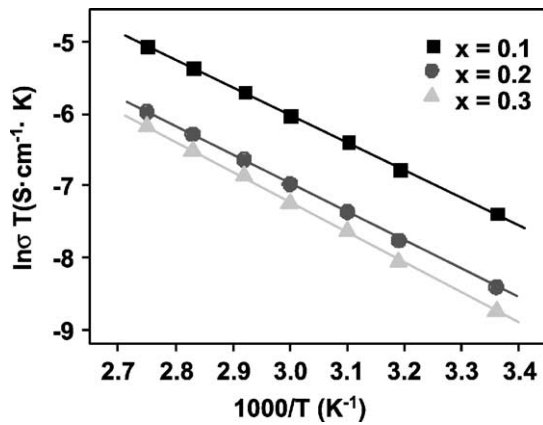


Fig. 5. Logarithmic plot of ionic conductivity as inverse function of temperature $1000/T$ for $\text{Li}_x\text{B}_{1-x/3}\text{PO}_4$.

Table 2

Activation energies and pre-exponential factors of $\text{Li}_x\text{B}_{1-x/3}\text{PO}_4$ for different lithium contents (x)

x	E_a (eV)	$\ln \sigma_0$ (S cm ⁻¹)
0.1	0.3039	-1.2447
0.2	0.3197	-1.6541
0.3	0.3385	-1.2562

over the entire temperature range. The activation energies and pre-exponential factors of $\text{Li}_x\text{B}_{1-x/3}\text{PO}_4$ are listed in Table 2. The activation energy increase from 0.3039 to 0.3385 eV with increasing lithium content. This trend is most likely due to a decrease in the bottleneck size present in the $(0k0)$ direction [11]. The pre-exponential factors related to the mobile ion concentration do not change with lithium content x . This suggests that activation energy is one of the main factors that control the ionic conductivity in $\text{Li}_x\text{B}_{1-x/3}\text{PO}_4$.

4. Conclusion

In defect models, it is thought that the conduction mechanism of $\text{Li}_x\text{B}_{1-x/3}\text{PO}_4$ is the migration of interstitial lithium ions through boron vacancies. The activation energy for lithium ion conduction increases from 0.3039 to 0.3385 eV with increasing lithium content. When the activation energy is low, lithium ions can migrate more easily and the ionic conductivity of $\text{Li}_x\text{B}_{1-x/3}\text{PO}_4$ improves. When the activation energy is at its minimum value the maximum ionic conductivity is $3.74 \times 10^{-6} \text{ S cm}^{-1}$ at room temperature for $x = 0.10$.

Acknowledgements

This work was supported by KOSEF through the Research Center for Energy Conversion and Storage.

References

- [1] M. Duclot, J.-L. Souquet, J. Power Sources 97–98 (2001) 610–615.
- [2] E.M. Kelder, M.J.G. Jak, F. de Lange, J. Schoonman, Solid State Ionics 85 (1996) 285–291.
- [3] M.J.G. Jak, E.M. Kelder, M. Stuiyinga, J. Schoonman, Solid State Ionics 86–88 (1996) 897–902.
- [4] G.E. Schulze, Z. Phys. Chem. B 24 (1934) 215.
- [5] A. Adamczyk, M. Handke, J. Mol. Struct. 555 (2000) 159–164.
- [6] M.J.G. Jak, E.M. Kelder, J. Schoonman, J. Solid State Chem. 142 (1999) 74–79.
- [7] M.J.G. Jak, V.W.J. Verhoreven, I.M. de Schepper, F.M. Mulder, E.M. Kelder, J. Schoonman, Physica B 266 (1999) 108–111.
- [8] E. Gruner, Z. Anorg. Allg. Chem. 219 (1934) 181.
- [9] M.J.G. Jak, E.M. Kelder, S.J. Everstein, J. Schoonman, J. Power Sources 81–82 (1999) 808–812.
- [10] R. Kanno, T. Hata, Y. Kawamoto, M. Irie, Solid State Ionics 130 (2000) 97–104.
- [11] M.G.J. Jak, E.M. Kelder, Z.A. Kaszkur, J. Pielaszek, J. Schoonman, Solid State Ionics 119 (1999) 159–164.